

EFFECTS OF HELICOPTER ROTOR WAKE CHARACTERISTICS ON BLADE AIRLOADS

X. K. Zioutis, A. I. Spyropoulos, D. P. Margaritis, D. G. Papanikas
Fluid Mechanics Lab., Mechanical Engineering. and Aeronautics Department,
University of Patras, Greece

Keywords: *helicopter aerodynamics, rotor wake, core model*

Abstract

Several research efforts have been recently conducted, aiming to improve the physical understanding and predictive capabilities of the complicated helicopter rotor flowfield. As a result, advanced mathematical models have been developed, targeting to enhance the aerodynamic computations of rotor wake analysis.

The implementation of these mathematical models is presented here, in a developed computational procedure, based on a Lagrangian type, Vortex Element Method. The free vortical wake geometry and rotor airloads are computed. The computational efficiency of special models concerning vorticity diffusion and vortex straining is tested. An investigation regarding the benefit of using curved line segments instead of straight ones, in spite their computational cost, is made with the developed wake relaxation method.

The results of curved segments application, combined with concepts engaged for straight segments such as vortex core models, have been computationally evaluated. Investigations have also been performed in order to assess a realistic value for empirical factors included in vorticity diffusion models.

The computational results are compared with experimental data from wind tunnel tests, performed during joined European research programs.

1 Introduction

During recent years computational research, free vortex methods have been established as a

reliable tool for computing the non-uniform induced downwash of a lifting helicopter rotor [1,2]. The reason for this development is that the above methods can computationally reproduce an accurate geometry of the concentrated wake vortices spinning close to rotor disk, which are responsible for the rotor blade vibratory airloads. From the first simplified approaches [3,4], to recent advanced procedures [5-9], rotor wake vortices have been simulated by concentrated vorticity elements such as vortex lines and vortex sheets [5,10].

The above Vortex Element Methods (VEM), analyze rotor wake with sophistication level ranging from preliminary to advanced manufacture calculations. The basic formulation of VEM is closely related to classical vortex methods for boundary layer and vortical flow analysis extensively applied by Chorin [11], Leonard [12] and other researchers [13].

Computational research on helicopter rotor focuses on blade airloads prediction, trying to identify the effects on blade vibrations and noise emissions of many structural and flowfield parameters such as wake formation, blade planform, flight conditions etc. To achieve this, Lagrangian type methodologies have been developed which combine VEM for the vortical wake representation, with a lifting line or surface method for rotor blade calculations. Usually an iterative scheme is used, where successive wake and rotor calculations lead to solution convergence. The wake vortices are considered free to move, under the influence of their self-induced velocity field, either by externally imposing geometrical periodicity (relaxation methods) or not (time marching methods). Thus this free-wake concept leads to

a non-uniform induced downwash on rotor blades, which is responsible for radial and azimuthal blade airload fluctuations.

Different physico-mathematical models for some special aerodynamic phenomena in rotor blade and wake flowfield, have a significant influence on computed blade airload distributions. Therefore an extensive effort is made by several researchers to investigate, among others, the appropriate model for simulating viscous vortex core structure, vorticity diffusion, trailing vortex rollup process, rotor blade dynamic stall and other phenomena [14].

In the work presented here a Lagrangian method of the wake-relaxation type is employed [15,16], to investigate the influences of specific aerodynamic models on blade airloading. The applied method consists of a free wake analysis which employs VEM and a coupled airload computation module which has the flexibility to adopt either lifting line or lifting surface methods. Blade motion calculations include provisions for articulated or hingeless blades and the main rigid and elastic flapping modules can be regarded separately or coupled.

Line segment discretization of wake vortices has prevailed when helicopter rotor wakes are simulated. This is because velocity induced to any point in wake or rotor flowfield can be readily computed by integrating Biot-Savart law in closed form over each segment. Methods with straight [8,10] or curved [6,17] line segments have been proposed and their accuracy was found to be of second order comparing to vortex ring analytical solution [18,19]. Rarely, the distributed vorticity behind the inner part of blade span is modeled by surface elements such as vortex sheets [10]. For the present investigation, a model of multiple trailing lines is adopted and compared with models engaging three trailing lines or vortex sheets. Comparison between straight line and curved line segmentation of wake vortices is performed, in order to investigate the effectiveness of curved elements despite their increased computational demands.

Viscous effects on wake vorticity have also been the subject of computational and

experimental efforts because of their significant impact on induced velocity calculations especially for large wake ages [20-22]. These effects are the vortex core formation in the center of vortex lines, where the circumferential velocity tends to zero and the diffusion of the concentrated vorticity as time progresses. Both of these phenomena are found to be of crucial importance for a reliable wake representation. Several models are compared, assuming both laminar and turbulent vortex core flow, in order to demonstrate their effectiveness and a parametric investigation is performed concerning empirical factors employed by these models.

The experimental data used for comparisons include test cases executed during cooperative European research programs on rotorcraft aerodynamics and aeroacoustics performed in the open test section of the German-Dutch Wind Tunnel (DNW) The Netherlands [23].

2 Aerodynamic formulation

2.1 Rotor wake model

The vorticity in rotor wake is distinguished by VEM regarding its source in two main parts, the trailing and the shed vorticity. Conservation of circulation dictates that vorticity shed at specific spanwise locations behind each blade is determined by circulation gradients on the blade. Spanwise circulation variations on rotor blade generate trailing vorticity, g_n , whose direction is parallel to the local flow velocity (Figure 1). On the other hand, azimuthal variations produce shed vorticity radially oriented, g_s , due to the transient periodical nature of the rotor blade flowfield.

In general, bound circulation has a distribution as shown in Figure 1, where the pick is located outboard of the semi-span and there is steep gradient near the blade tip, responsible for the formation of a strong vortex at the tip.

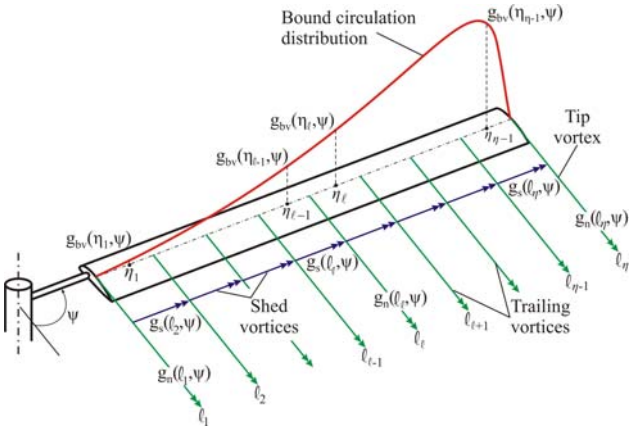


Fig. 1. Modeling of rotor blade bound circulation distribution and wake vorticity formations.

The scope of VEM is to represent these two kinds of vorticity with simple computational elements, in order to predict the velocity field induced on the rotor disk and in the wake itself. For this purpose discrete straight or curved line vortex segments are used.

The first step at the present analysis is to simulate trailing vorticity by n-straight line vortex segments, labeled ℓ_ℓ , which run from ℓ_1 at the root to ℓ_n at the tip. Special care has been given for the tip vortex representation, which may be simulated either by straight or curved line vortex segments as described in the next paragraph. The bound circulation is known at $\eta_\ell = n-1$ radial stations, where η_ℓ runs from η_1 between ℓ_1 and ℓ_2 to η_{n-1} between ℓ_{n-1} and ℓ_n . Now, the strength of each segment is equal to the gradient of the bound circulation g_{bv} between two successive radial stations. This means that for all intermediate segments:

$$g_n(\ell_\ell, \psi) = g_{bv}(\eta_{\ell-1}, \psi) - g_{bv}(\eta_\ell, \psi) \quad (1)$$

The first term is equal to zero at the root the, because there is no bound circulation inboard the root. Analogically the second term is zero at the tip.

The shed vorticity is simulated by n-1 straight line vortex segments which are extended radially between two adjacent trailing vortices as shown at Figure 1. The strength of each segment is equal to the azimuthal variation of bound circulation for each radial station:

$$g_s(\ell_\ell, \psi) = g_{bv}(\eta_{\ell-1}, \psi + \Delta\psi) - g_{bv}(\eta_{\ell-1}, \psi) \quad (2)$$

The table of Figure 2 shows three different wake models which are tested for the representation of rotor wake. The resulting azimuthal distribution of normal force coefficient C_N is compared with experimental data in Figure 3.

Wake Model	Shed Wake	Inboard Wake	Tip Vortex
1	50 SLV	50 SLV	1 SLV
2	1 SLV	VS	1 SLV
3	VS	VS	1 SLV

Fig. 2. Table of wake models for rotor wake simulation. SLV = Straight Line Vortex VS = Vortex Sheet

As shown in this figure, representing the total rotor wake with n-straight line vortices is preferable than using vortex sheets for trailing or shed wake. For this reason wake model 1 is used hereafter for the simulation of rotor wake.

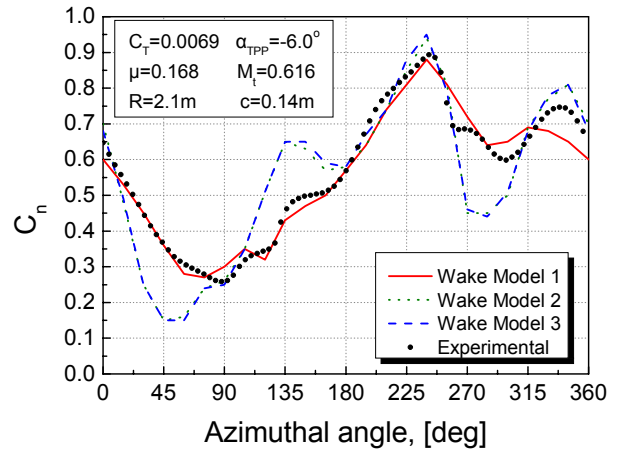


Fig. 3. Comparison of the wake model influences at radial station 0.82 for a climb case.

2.2 Induced velocity calculation

The utilization of discrete computational elements by VEM for rotor wake simulation, converts direct integration in a closed form integration of the Biot-Savart law over the known spatial locations of these elements. Two different types of vortex elements, straight-line and curved, have been used to simulate the rotor

wake. The contribution of a straight-line vortex segment to the induced velocity can be found in [15].

The use of straight-line vortex segments constitutes a geometric approximation of the vortex curve. As shown at Figure 4, the errors associated with straight-line vortex segments can be classified as position errors δ_{SL} and curvature errors [17].

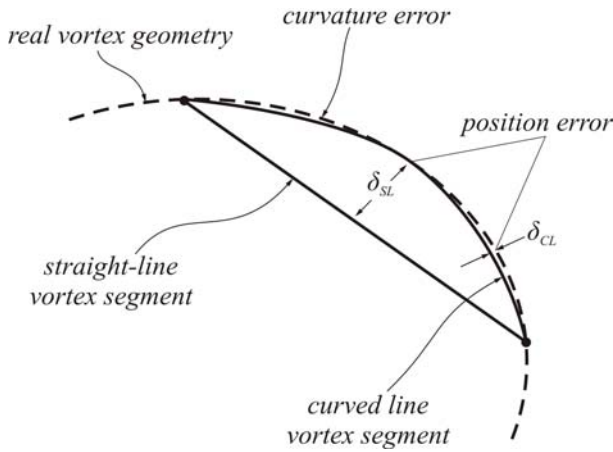


Fig. 4. Position and curvature errors by straight and curved line vortex segment.

In order to reduce these errors, the use of curved line vortex segments and specifically of parabolic arcs has been tested. Figure 5 shows a parabolic arc defined by the equation $y_\ell = \epsilon x_\ell^2$ having circulation Γ , which may vary along the arc. The induced velocity is calculated at point P_η , which lies at distance \vec{r} from the incremental length $d\vec{\sigma}$.

Integration of the Biot-Savart law over the arc C assuming linear variation of the circulation $\Gamma(x_\ell) = \Gamma_o + \Gamma_1 x_\ell$, yields the following results:

$$q_x = \frac{\epsilon \Gamma_o z}{2\pi} I_1 \Big|_C + \frac{\epsilon \Gamma_1 z}{2\pi} I_2 \Big|_C \quad (3)$$

$$q_y = -\frac{\Gamma_o z}{4\pi} I_0 \Big|_C - \frac{\Gamma_1 z}{4\pi} I_1 \Big|_C \quad (4)$$

$$q_z = \frac{y \Gamma_o}{4\pi} I_0 \Big|_C - \frac{[2\epsilon \Gamma_o x - y \Gamma_1]}{4\pi} I_1 \Big|_C - \frac{[2\epsilon \Gamma_1 x - \epsilon \Gamma_o]}{4\pi} I_2 \Big|_C + \frac{\epsilon \Gamma_1}{4\pi} I_3 \Big|_C \quad (5)$$

The integrals of the preceding equations are of the form

$$I_n = \int \frac{x_\ell^n}{[c x_\ell^2 + b x_\ell + a]^{3/2}} dx_\ell \quad (6)$$

and their values for $n=0, 1, 2, 3$ can be found in [24].

A special procedure is required to connect curved line vortex segments in order to form a continuous vortex curve, which is not needed for straight line segments. At the present work an intermediate point is computed within each interval between two collocation points.

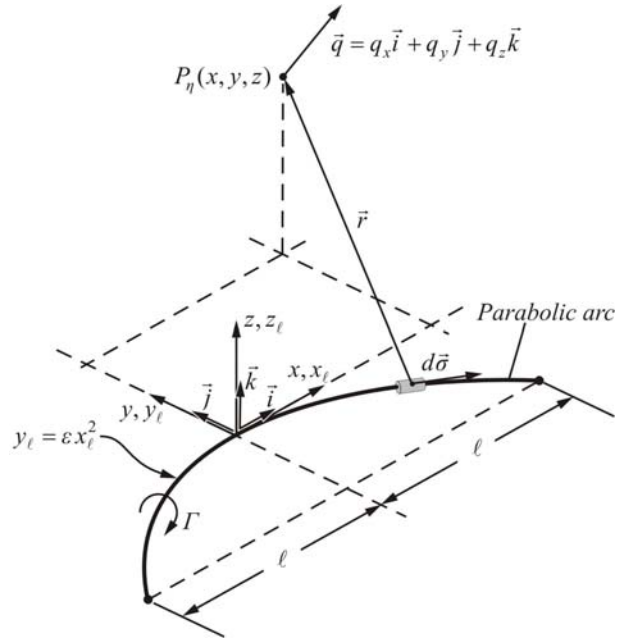


Fig. 5. Parabolic arc geometry for the Biot-Savart integration.

2.3 Vortex core structure

VEM is based on potential field solution such as Biot-Savart law for the calculation of the velocity induced by vortex elements. Due to the absence of viscosity, the induced velocity calculated by the Biot-Savart law on a point lying very close to a vortex segment, tends to be

infinite which is unrealistic. In order to remove these singularities and model the effects of viscosity in a convenient way the vortex core concept is introduced.

Several algebraic models for the vortex induced velocity have been introduced due to their simplicity and computational efficiency in engineering applications [25-27]. One of the most commonly used models is the model suggested by Scully and Sullivan [28] and also by Kauffman [29]. A series of tangential velocity profiles was also proposed by Vatisias [30]. Taking these models into account, the present investigation also applies the Rotary Wing vortex model [10] and of the Lamb-Oseen model [31] for the representation of the vortex core structure.

2.4 Core growth

Unlike airplanes, helicopter rotors remain in close proximity to their tip vortices, more so in descent and maneuvers. This unique characteristic leads to close encounters of rotor blades with tip vortices, which are known as blade vortex interactions or BVIs. As a consequence, an understanding of not only the initial core size after roll-up but also the subsequent growth of the vortex core is important [32].

The effect of diffusion on the growth of properties of the tip vortices is taking into account by increasing the vortex core radius and decreasing its vorticity as time increasing. The simplest viscous vortex is the Lamb-Oseen vortex model. This is a two-dimensional flow with circular symmetry in which the streamlines are circles around the vortex filament and the vorticity is a function of radial distance r and time t and parallel to the vortex filament. Solving the Navier-Stokes equations for this case an exact solution for the tangential or swirl velocity surrounding the vortex filament arises as

$$V_{\theta}(r) = \frac{\Gamma_{TIP}}{2\pi r} \left(1 - e^{-r^2/4vt}\right) \quad (7)$$

where Γ_{TIP} is the tip vortex strength and ν is the kinematic viscosity.

The core growth with time, predicted by the Lamb-Oseen model is given by

$$r_{diff}(t) = 2.24181\sqrt{vt} \quad (8)$$

This result came up by differentiating eq. (7) with respect to r and setting the derivative to zero. The Lamb-Oseen vortex can be regarded as the “desingularisation” of the rectilinear line vortex, in which the vorticity has a delta-function singularity.

Squire [33] showed that the solution for a trailing vortex is identical to the Lamb-Oseen solution. So the downstream distance z from the origin of the vortex can be related to time as $t=z/V_{\infty}$. In order to account for effects on turbulence generation, Squire introduced an eddy viscosity coefficient δ . In the case of a helicopter rotor, time t is related to the wake age δ_{ℓ} as $\delta_{\ell} = \Omega t$, where Ω is the angular velocity of the rotor. Thus, including these parameters eq. (8) can be written as

$$r_{diff}(\delta_{\ell}) = 2.24181\sqrt{\delta\nu\left(\frac{\delta_{\ell} + \delta_0}{\Omega}\right)} \quad (9)$$

In the above equation δ_0 is an effective origin offset, which gives a finite value of the vortex core radius at the instant of its generation ($\delta_{\ell}=0$) equals to

$$r_{diff}(\delta_{\ell} = 0) \equiv r_0 = 2.24181\sqrt{\delta\nu\left(\frac{\delta_0}{\Omega}\right)} \quad (10)$$

At this work δ_0 was selected to have an age between 15° and 30° .

According to Squire, the eddy viscosity coefficient is proportional to the vortex Reynolds number Re_v and equals to

$$\delta = 1 + \alpha_s Re_v \quad (11)$$

where α_s is the Squire’s parameter and its value is determined from experimental measurements.

A phenomenon often opposing vortex diffusion is the straining of vortex filaments due to their freely distorted geometry. In fact the steep gradients of wake induced velocities cause them to stretch or to squeeze and their core radius to decrease or to increase

correspondingly. These effects are independent of diffusion and can be observed even when diffusion is omitted.

In order to include straining effects, define

$$\varepsilon = \frac{\Delta\ell}{\ell} \quad (12)$$

as the strain imposed on the filament over the time interval Δt , where $\Delta\ell$ is the deformation from its initial length ℓ . Now assume that the filament has a core radius $r_{diff}(\delta_\ell)$ at time δ_ℓ . At time $\delta_\ell + \Delta\psi$ the filament will have a core radius $r_{diff}(\delta_\ell + \Delta\psi) - \Delta r_{diff}(\delta_\ell) = r_{strain}$ because of straining. Applying the principle of conservation of mass leads to the following result

$$r_{strain}(\delta_\ell + \Delta\psi) = r_{diff}(\delta_\ell) \frac{1}{\sqrt{1 + \varepsilon}} \quad (13)$$

Combining equations (9) and (13) a vortex core radius including both diffusion and straining effects can be defined as

$$\begin{aligned} r_c(\delta_\ell) &= r_{diff}(\delta_\ell) - r_{strain}(\delta_\ell) \\ &= r_{diff}(\delta_\ell) - r_{diff}(\delta_\ell - \Delta\psi) \frac{1}{\sqrt{1 + \varepsilon}} \end{aligned} \quad (14)$$

3 Results and discussion

Tip vortex is the dominant part of rotor wake as the source of vibratory airloads and phenomena such as BVI or the aeroacoustic noise. For this reason its representation is crucial. Bliss [17] has introduced curved line vortex segments to simulate the tip vortex with higher accuracy than of the straight line vortex segments. However as showed in [18], the same accuracy can be achieved with the appropriate descritization using straight line vortex segments. Figure 6 compares the azimuthal variation of the normal force coefficient with experimental data. The computations were performed using curved and straight line vortex segments for the tip vortex. It is clear that both straight and curved lines give almost the same results, which confirm the observation in [18]. Having in mind the simplicity of straight line vortex segments it is much more convenient to

use them instead of curved.

As mentioned before in order to include diffusion effects in the vortex core, Squire's parameter a_s must be defined. For this purpose a computational investigation has been done for the derivation of an acceptable value of a_s . Figure 7 shows the azimuthal distribution of the normal force coefficient for several values of a_s varying from 10^{-1} to 10^{-5} . Comparing the computed results with the corresponding experimental, a value of the order of 10^{-4} to 10^{-5} , from diagrams (d) and (e), seems to be best for the current data. This value for a_s has also been suggested by Leishman [34]. At this work a value of 0.000065 was selected for a_s as shown in diagram (f) of Figure 7.

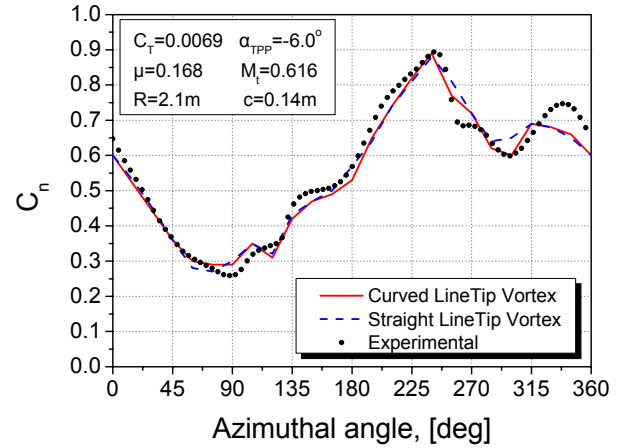


Fig. 6. Comparison of curved and straight line tip vortex segments effects on rotor computations.

Having found an appropriate value for a_s , several core models are applied to simulate the tip vortex core structure for both straight and curved line vortex segments. Figures 8a and 8b show that the last three core models give about the same results. This is expected because these models were obtained from the same series family proposed by Vatisstas. For the straight line tip vortex representation (Figure 8a) the Lamb-Oseen core model is slightly better than the others, while for the curved line tip vortex representation (Figure 8b) the Rotary Wing seems to give better results for this test case. Comparing the diagrams of Figure 8a and 8b the Rotary Wing core model seems to be “steady”, while the other three models give different results for straight and curved lines. This information can be useful for the computational

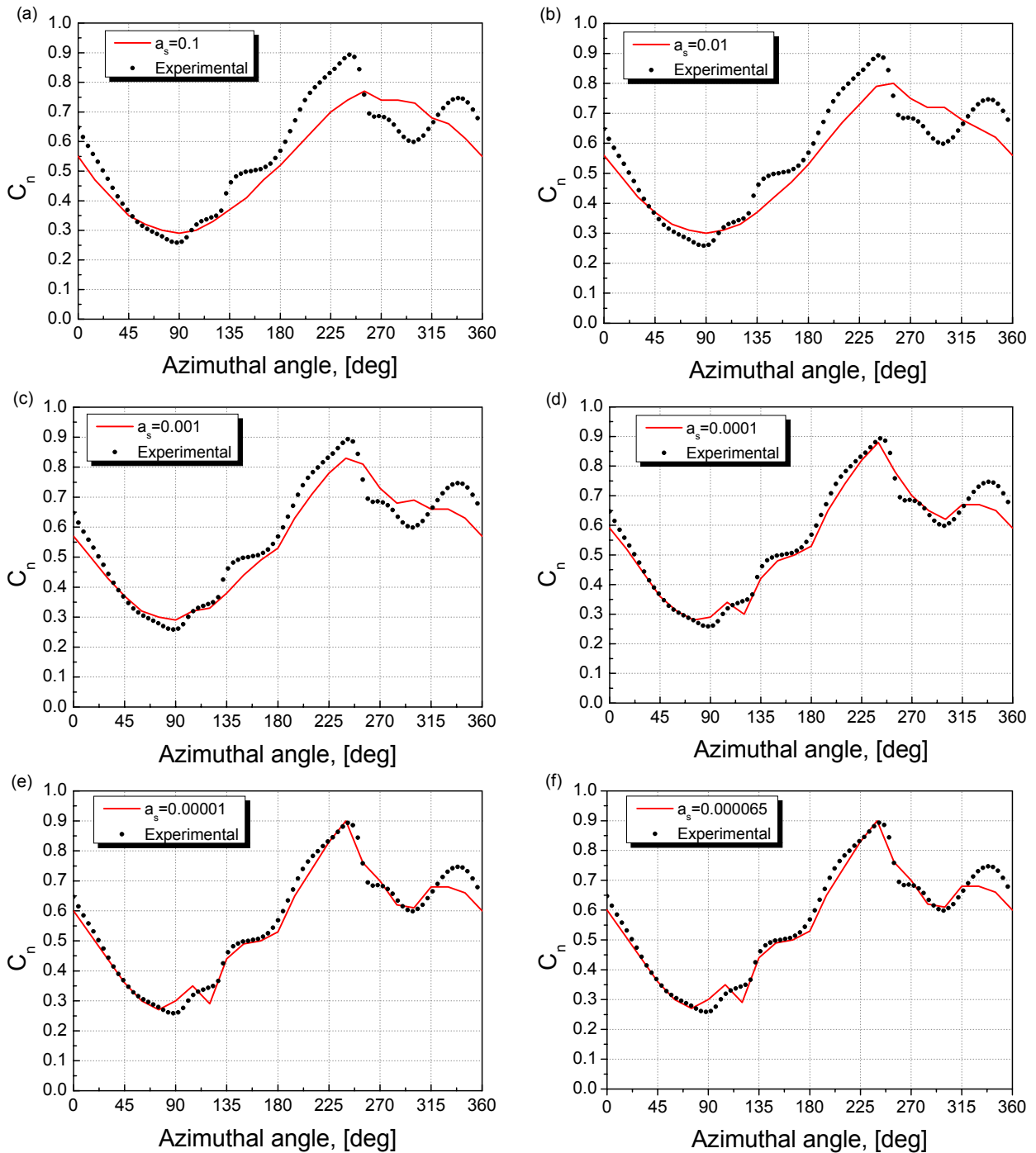


Fig. 7. Computational investigation for the definition of Squire's parameter a_s .

comparison of the straight and curved line vortex segments.

The importance of diffusion effects was also studied. Using the Lamb-Oseen model for the straight line tip vortex core structure, a comparison is made between experimental and computed C_N for the cases where diffusion effects are included and neglected respectively. The diagram of Figure 9 shows that better

results are obtained when diffusion effects are included. This is evidence of the necessity to include tip vortex core diffusion in order to get more realistic results. For the same case, Figure 10 shows two contours of the downwash produced, when diffusion effects are included and neglected.

An effort was also made in order to include straining effects at the tip vortex core growth.

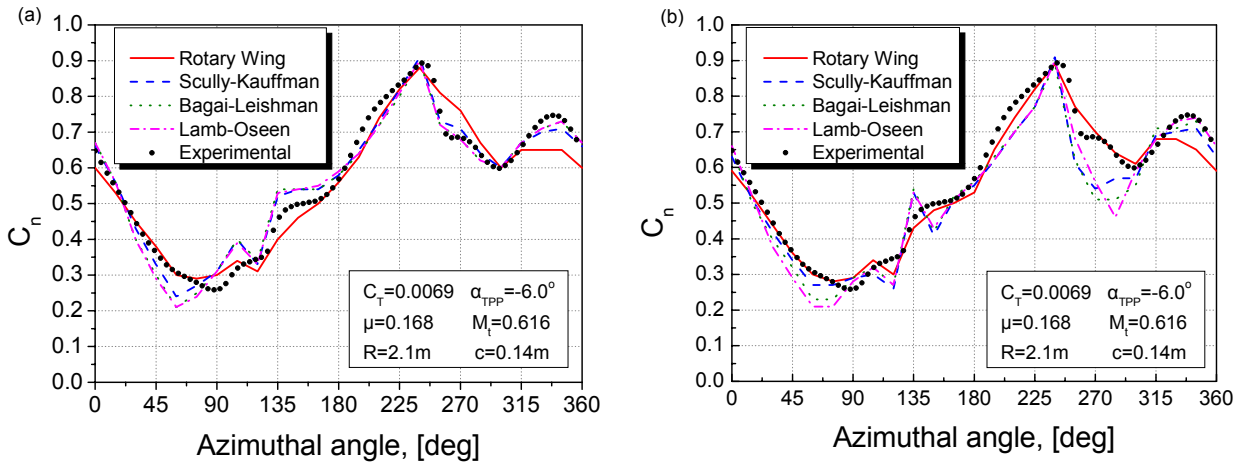


Fig. 8. Vortex core model comparison for the cases where the tip vortex is simulated (a) by straight line vortex segments, (b) by curved line vortex segments.

This phenomenon is often opposing diffusion as has already been mentioned. Figure 11 shows the computed azimuthal distribution of C_N for the cases where straining effects are included and neglected respectively. The results are compared with experimental data. For the current test case it seems that straining effects do not play an important role as diffusion.

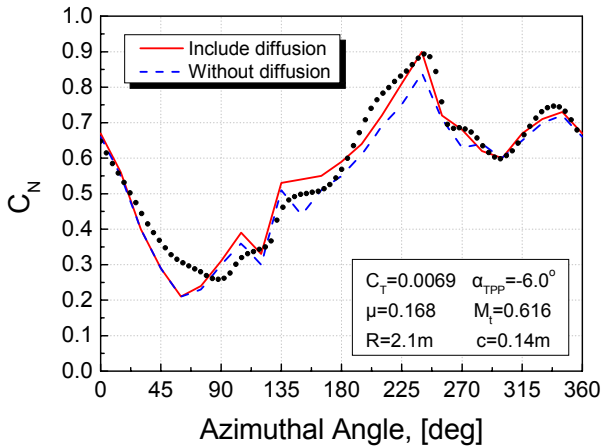


Fig. 9. Comparison of experimental and computed C_N when diffusion effects are included and neglected respectively.

4 Conclusions

A model for the simulation of rotor wake has been developed using n -trailing vortex lines. Special care has been given for the tip vortex which can be represented either by straight or curved line vortex segments. Diffusion and straining effects of the tip vortex have been

appropriate simulated in order to investigate their influences. To include viscous effects

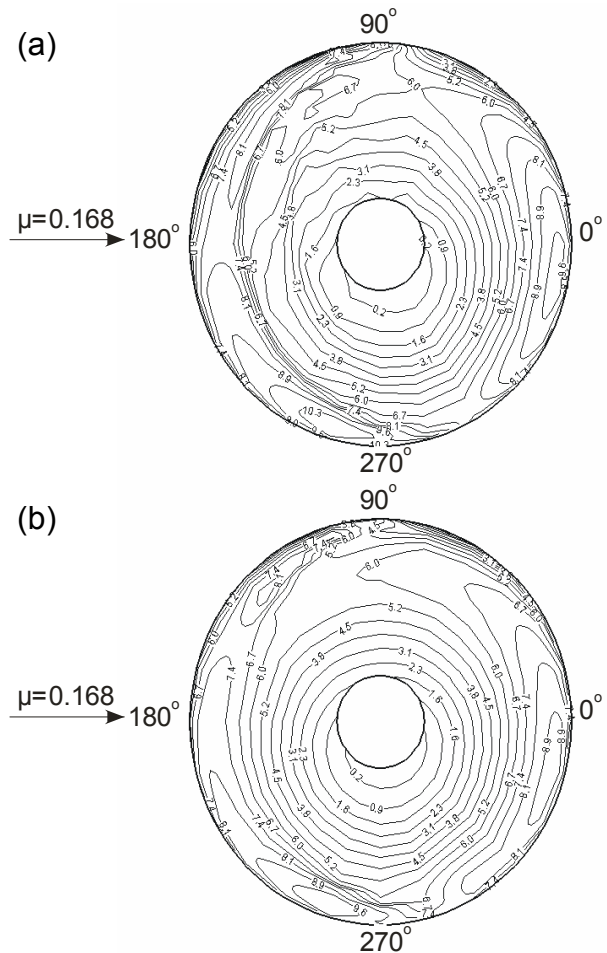


Fig. 10. Non-uniform downwash, calculated when diffusion effects are (a) included (b) neglected

several core models have been tested.

The conclusions from this study are

summarized as follows:

1. Simulating the rotor wake by n-straight line vortices is preferable than using vortex sheets to simulate the inboard or the shed wake.
2. Both straight and curved lines vortex segments gave almost the same results. However because of their simplicity straight line vortex segments are much more convenient instead of curved.
3. Squire's parameter a_s has been found to be of the order of 10^{-4} to 10^{-5} . At this work a value equals to 0.000065 was selected.
4. Straining effects do not take place important role as diffusion.

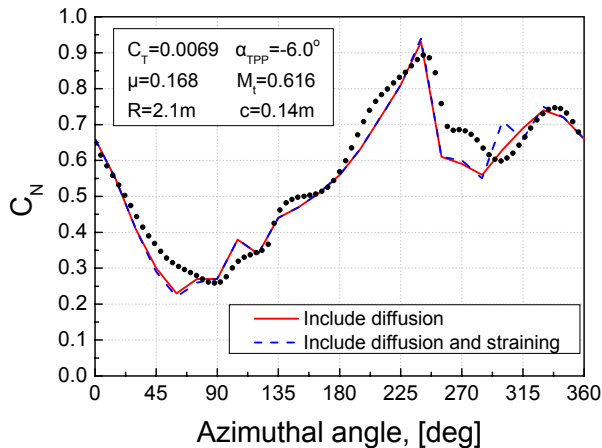


Fig. 11. Comparison of experimental and computed C_N when straining effects are included and neglected respectively.

References

- [1] Johnson W. Rotorcraft aerodynamics models for a comprehensive analysis. *Proceedings of 54th Annual Forum of American Helicopter Society*, Washington, DC, May 20-22, 1998.
- [2] Leishman G J, Bhagwat M J and Bagai. A. Free-vortex filament methods for the analysis of helicopter rotor wakes. *Journal of Aircraft*, Vol. 39, No. 5, pp 759-775, 2002.
- [3] Egolf T. A., and Landgrebe A. J. A prescribed wake rotor inflow and flow field prediction analysis. *NASA CR 165894*, June 1982.
- [4] Beddoes T S. A wake model for high resolution airloads. *Proceedings of the 2nd International Conference on Basic Rotorcraft Research*, Univ. of Maryland, College Park, MD, 1985.
- [5] Bhagwat M J and Leishman G. J. Stability, consistency and convergence of time-marching free-vortex rotor wake algorithms. *Journal of American Helicopter Society*, Vol. 46, No. 1, pp. 59-71, 2001.
- [6] Quackenbush T R, Wachspress D A and Boschitsch. Rotor aerodynamic loads computation using a constant vorticity contour free wake model. *Journal of Aircraft*, Vol. 32, No. 5, pp. 911-920, 1995.
- [7] Chua K. and Quackenbush T. R. Fast three-dimensional vortex method for unsteady wake calculations. *AIAA Journal*, Vol. 31, No. 10, pp. 1957-1958, 1993.
- [8] Bhagwat M. J. and Leishman G. J. Rotor aerodynamics during manoeuvring flight using a time-accurate free vortex wake. *Journal of American Helicopter Society*, Vol. 48, No. 3, pp. 143-158, 2003.
- [9] Xu G. H. and Newman S. J. Helicopter rotor free wake calculations using a new relaxation technique. *Proceedings of 26th European Rotorcraft Forum*, Paper No. 37, 2000
- [10] Scully M P. Computation of helicopter rotor wake geometry and its influence on rotor harmonic airloads. *ASRL TR 178-1*, 1975
- [11] Chorin A. J. *Computational fluid mechanics*. 1st edition, Academic Press, 1989
- [12] Leonard T. Computing three dimensional incompressible flows with vortex elements. *Annual Review of Fluid Mechanics*, Vol. 17, pp. 523-559.
- [13] Sarpkaya T. Computational methods with vortices - The 1988 Freeman scholar lecture. *ASME Journal of Fluids Engineering*, Vol. 111, No. 5, March 1989.
- [14] Hariharan N. and Sankar L. N. A review of computational techniques for rotor wake modelling. *Proceedings of AIAA 38th Aerospace Sciences Meeting*, AIAA 00-0114, Reno NV, 2000.
- [15] Spyropoulos A. I, Fragias A. P., Papanikas D. G. and Margaris D. P. Influence of arbitrary vortical wake evolution on flowfield and noise generation of helicopter rotors. *Proceedings of the 22nd ICAS Congress*, Harrogate, United Kingdom, 2000.
- [16] Papanikas D G, Spyropoulos A I, Fertis D K and Margaris D P. Helicopter rotor downwash calculation using the vortex element method for the wake modelling. *Proceedings of the 20th ICAS Congress*, Sorrento, Italy, 1996.
- [17] Bliss D B, Teske M E and Quackenbush T R. A new methodology for free wake analysis using curved vortex elements. *NASA CR-3958*, 1987.
- [18] Gupta S. and Leishman G. J. Accuracy of the induced velocity from helicoidal vortices using straight-line segmentation. *AIAA Journal*, Vol. 43, No.1, pp 29-40, 2005.
- [19] Wood D. H. and Li D. Assessment of the accuracy of representing a helical vortex by straight segments. *AIAA Journal*, Vol. 40, No.4, pp 647-651, 2005.
- [20] Ramasamy M., Leishman G. Interdependence of diffusion and straining of helicopter blade tip

- vortices. *Journal of Aircraft*, Vol. 41, No. 5, pp 1014-1024, 2004.
- [21] Tung C. and Ting L. Motion and decay of a vortex ring. *Physics of Fluids*, Vol. 10, No. 5, pp. 901-910, 1967.
- [22] Stott J. A and Duck P. W. The effects of viscosity on the stability of a trailing-line vortex in compressible flow, *Physics of Fluids*, Vol. 7, No. 9, pp. 2265-2270, 1995.
- [23] Spletstoeser W. R., Niesl G., Cenedese F., Nitti F. and Papanikas D. G. Experimental results of the European HELINOISE aeroacoustic rotor test. *Journal of American Helicopter Society*, Vol. 40, No.2, 1995.
- [24] Gradshteyn, I.S. and Ryzhik, I.W. *Tables of integrals, series and products*, 4th ed., Academic Press, 1965.
- [25] Windnall S. E. and Wolf T. L. Effect of tip vortex structure on helicopter noise due to blade vortex interactions. *AIAA Journal of Aircraft*, Vol. 17, No. 10, pp. 705-711, 1980.
- [26] Bhagwat J. M. and Leishman G. J. Correlation of helicopter rotor tip vortex measurements. *AIAA Journal*, Vol. 38, No. 2, pp. 301-308, 2000.
- [27] Vatistas G. H, Kozel V. and Mih W. C. A simpler model for concentrated vortices. *Experiments in Fluids*, Vol. 11, pp.73-76, 1991.
- [28] Scully M. P. and Sullivan J. P. *Helicopter rotor wake geometry and airloads and development of laser Doppler velocimeter for use in helicopter rotor wakes*. Massachusetts Institute of Technology Aerophysics Laboratory Technical Report 183, MIT DSR No. 73032, 1972.
- [29] Kaufmann, W. Uber die ausbreitung kreiszylindrischer wirbel in zahn flussigkeiten, *Ing. Arch.*, Vol. 31, No. 1, 1962.
- [30] Vatistas G. H, Kozel V. and Mih W. C. A simpler model for consebrated vortices. *Experiments in Fluids*, Vol. 11, pp. 73-76, 1991.
- [31] Batchelor G. K., *Introduction to fluid dynamics*. Cambridge University Press, 1967.
- [32] Zioutis X. K., Spyropoulos A. I., Margaritis D. P. and Papanikas D. G. Numerical investigation of BVI modelling effects on helicopter rotor free wake simulations. *Proceedings of the 24th ICAS Congress*, 2004, Yokohama, Japan.
- [33] Squire, H. B. The growth of a vortex in turbulent flow, *Aeronautical Quarterly*, Vol. 16, August 1965, pp.302-306.
- [34] Bhagwat J. M. and Leishman G. J. Generalized viscous vortex model for application to free-vortex wake and aeroacoustic calculations, *Proceedings of American Helicopter Society 58th Annual Forum and Technology Display*, Montreal, Canada, 2002.